Mechanics of Microtubule Bundles in Pillar Cells from the Inner Ear

J. A. Tolomeo and M. C. Holley
Department of Physiology, University of Bristol, Bristol BS8 1TD, England

ABSTRACT The mechanical properties of cross-linked microtubule bundles were measured from outer pillar cells isolated from the mammalian inner ear. Measurements were made using a three-point bending test and were incorporated into a mathematical model designed to distinguish between the stiffness contributions from microtubules and their cross-linking proteins. Outer pillar cells were composed of 1000–3000 parallel bundled microtubules in a square array that was interdigitated and cross-linked with actin filaments. The average midpoint bending stiffness of intact cells was 7×10^{-4} N/m. After removal of both the actin filaments and cross-links with detergent in the presence of DNase I, the square array was disrupted and the stiffness decreased by a factor of 4, to 1.7×10^{-4} N/m. The bending modulus for individual microtubules was calculated to be 7×10^{-23} Nm^2, and the Young's modulus for these 15 protofilament microtubules was 2×10^9 Pa. The shear modulus between microtubules in intact cells was calculated to be 10^3 Pa. It was concluded that cross-linking proteins provided shear resistance between microtubules, which resulted in a fourfold increase in stiffness. The model can be used to estimate the mechanical properties of cross-linked microtubule bundles in cells from which direct measurements are not available.

INTRODUCTION

Outer pillar cells (OPCs) from mammalian auditory sensory epithelia are ideal for direct measurement of the structural and material properties of microtubules and their cross-linking proteins. They possess a cytoskeleton composed of thousands of parallel, cross-linked microtubules and actin filaments. Two additional types of supporting cells, namely inner pillar cells and Deiter's cells, possess similar, if slightly less organized, cytoskeletal bundles. Their main function is to provide cellular mechanical coupling between the mechanosensory hair cells and the basilar membrane.

OPCs differ from the other supporting cells because they stand as individual structures free from contact with adjacent cells, except at their bases and apices (Iurato, 1961; Angleborg and Engström, 1972). The main shaft broadens out at the base, where a dense cytoskeletal cone of actin forms a footplate on top of the basilar membrane. At the apex it is embedded in a dense plate of short, cross-linked actin filaments within which the microtubules terminate. A much shorter, narrower bundle of microtubules extends perpendicularly from this apical plate, runs along the epithelial surface, and attaches directly to the apex of a second-row outer hair cell.

The number of microtubules within the shaft of an OPC changes progressively with frequency location along the cochlea, and both the number and diameter of microtubules vary between species (Iurato, 1961; Angleborg and Engström, 1972; Kikuchi et al., 1991). In guinea pigs, microtubules are ~27–30 nm in diameter, with an inner diameter of ~13–17 nm. They are composed of 15 protofilaments rather then the more common number of 13 (Angleborg and Engström, 1972; Saito and Hama, 1982). Transverse sections through the shafts of OPCs show that the microtubules have a square packing, with an average center-to-center distance of ~42 nm (Iurato, 1961). Actin filaments lie between and in parallel with the microtubules (Slepecky and Chamberlain, 1983) and are cross-linked to the microtubules by short filaments less than 4 nm in diameter (Arima et al., 1986). A possible candidate for the cross-linking protein is a 205-kDa microtubule-associated protein (MAP) identified by immunocytochemistry (Oshima et al., 1992).

Several proteins cross-link microtubules with actin and promote bundle formation in vitro (Griffith and Pollard, 1982; MacRae, 1992). However, the mechanical effect of cross-linking in terms of bundle rigidity has not been measured or quantified. Our aim in this work was to measure how much of the stiffness of a microtubule bundle is due to the material properties of microtubules and how much to the cross-linking proteins. Measurements of bending rigidity were made from intact and sequentially extracted OPCs. The results are interpreted within a shear-weak filament composite analysis to calculate the apparent Young's modulus and shear modulus of the cytoskeleton. The mathematical model should allow a systematic prediction of the mechanical properties of similar cytoskeletal structures within other cells, including Deiter's cells in the organ of Corti, from which direct measurements cannot easily be made.

MATERIALS AND METHODS

Mechanical measurements

A three-point bending test was employed to measure cell stiffness as previously described for similar experiments on outer hair cells (Tolomeo

Received for publication 17 March 1997 and in final form 27 June 1997.

Address reprint requests to Dr. Matthew Holley, Department of Physiology, Medical Sciences, University Walk, Bristol BS8 1TD, England. Tel.: 117-9287811; Fax: 117-9288923; E-mail: m.c.holley@bristol.ac.uk.

Dr. Tolomeo's present address is Division of Mechanics and Computation, Department of Mechanical Engineering, Stanford University, Stanford, CA 94305.

0006-3495/97/10/2241/07 $2.00

et al., 1996). The glass measurement probe used throughout the experiments on pillar cells was 1 μm in diameter and had a tip stiffness of 4.5×10^{-4} N/m. The tip was melted before calibration to form a small bead about 3 μm in diameter. This served to improve contact with the microtubule bundles and to prevent the probe from slipping through the bundle. It also provided a well-defined image for video tracking. The calibrated probe tip was driven at 0.5 Hz and ~6 μm free displacement with a piezoelectric bimorph. Cells were viewed through a Nikon Diaphot inverted microscope. Video images were processed with an image enhancer (Brian Reece Scientific Ltd.) and recorded in real time on super VHS video. Quantitative analysis was performed by replaying the video through the image enhancer to imaging analysis software (Brian Reece Scientific Ltd.). Probe and cell deformation were tracked over 20 cycles while sampling 30 points per cycle. Fourier analysis and averaging were used to calculate the 0.5-Hz deformation signal. Error was calculated to be less than ±100 nm, as estimated by measuring the free displacement of the probe tip in air at different voltage steps and comparing this to the known linear range of operation for the piezo bimorph. All measurements were made from cells that were free from the surface of the slide.

Dissociation of intact cells

Dissociation of undamaged OPCs from the organ of Corti was essential for accurate mechanical estimates of cell stiffness. Guinea pigs were killed by cervical dislocation, and the bullae were removed and placed in Leibowitz L-15 (Gibco) solution. The bony exterior of the cochlea was opened, and the cochlear spiral was removed and incubated for 45 min in 3 mg/ml collagenase VIII (Sigma). The spiral was then placed in L-15 solution, and the pillar cells were dissociated by gently pipetting fluid over the organ of Corti. Cells were placed in 400 μl of L-15 containing enzyme inhibitors (100 μg/ml phenylmethylsulfonyl fluoride, 1 μg/ml pepstatin, 1 μg/ml leupeptin, and 2 mM benzamidine). Cells treated with DNase I were measured in both the presence and absence of these inhibitors. Rhodamine-labeled phalloidin was added at 0.1 μg/ml in the bathing solutions throughout the dissection as a test for cell damage. If at any stage the cell membrane was punctured, even if it subsequently resealed, it could be detected by fluorescence labeling of the intracellular actin filaments.

Extraction of cytoskeletal components

Cells were considered to be undamaged if they excluded phalloidin and possessed the expected morphology, an unbroken plasma membrane and a nucleus. Punctured cells retained their general morphology but did not possess an obvious plasma membrane or nucleus and labeled clearly with phalloidin. The plasma membrane and soluble cytoplasmic proteins were extracted with 0.2% Triton X-100. Filamentous actin was then extracted from the cell apices and shaft either by incubation with 0.1 mg/ml DNase I (Sigma), which selectively removes filamentous actin (Lazarides and Lindberg, 1974), or by labeling cells with rhodamine-phalloidin and then exposing them to a high-intensity ultraviolet light from an epifluorescence light source. The distribution of actin in intact cells was observed by labeling with rhodamine-phalloidin after fixation of dissociated cells with 4% paraformaldehyde.

Electron microscopy

A small opening was made in the cochlear shell to expose each turn of the cochlear spiral. The cochlear duct was then irrigated every 15 min with 2% ultrapure glutaraldehyde in a 0.1 M phosphate buffer (pH 7.4) and 1% tannic acid for 90 min. The spiral was then removed, washed in 0.1 M phosphate buffer every 5 min for 30 min, postfixed in 1% OsO_4 in 0.1 M phosphate buffer for 90 min, dehydrated through an ethanol series, permeated with propylene oxide, and embedded in Epon. To examine tissue extracted with 0.2% Triton, the spiral was removed, incubated three times for 5 min each in the same solution as that used for experimental measurement, and then fixed and embedded as above. All cochleae were cut into eight hemicoils with a 0.15-mm-thick diamond wafer blade, photographed, and reembedded. Thin sections of known orientation were stained with uranyl acetate and lead citrate and viewed with a Philips CM100 electron microscope.

RESULTS

Mechanical properties

Fig. 1 shows the morphology of intact and extracted cells. The stiffness of intact cells was measured as the ratio of the applied force to midpoint displacement as a function of the distance between fixed probes (Fig. 2). The data were plotted as a least-squares fit in a linear log-log form, giving an average midpoint stiffness of 7×10^{-4}N/m ($n = 21$, SD = $+5 \times 10^{-4}$, -3×10^{-4}, where the SD is symmetrical about the log-log linear form), with a length dependence that followed a power law slope of −2.3. The total length of intact OPCs ranged from ~75–110 μm, with an average length of 92 μm. This represents the full range of lengths occurring along the cochlear duct.

The entire shaft labeled with phalloidin in intact cells that were fixed with formaldehyde (not shown), but in punctured and Triton extracted cells the middle region of the shaft was unlabeled, suggesting that the filamentous actin had been lost (Fig. 1 *d*). The midpoint bending stiffness of punctured cells was less than that of intact cells by a factor of 2.6, with an average stiffness of 2.7×10^{-4} N/m ($n = 27$, SD = $+2.4 \times 10^{-4}$, -1.3×10^{-4}) and a power law slope of −2.4. Paired data for 13 cells were obtained by measuring intact cells before and after extraction with 0.2% Triton. The stiffness of 11 cells decreased to a stable value over several minutes, but for two there was little change. The average stiffness decreased by a factor of 2.0, very similar to that for punctured cells.

This decrease in stiffness may have been related to the loss of actin filaments, so further measurements were made from a population of cells that had been extracted with 0.2% Triton X-100 and 0.1 mg/ml DNase I. After 30 min of incubation, the microtubule bundles became optically less dense, although the microtubules themselves appeared to remain stable throughout the duration of the experiments. Without the beaded tip, the measurement probe readily passed between microtubules in the shaft, showing that they were not tightly bundled by cross-linking elements. The average midpoint stiffness was 1.7×10^{-4} N/m ($n = 37$, SD = $+1.2 \times 10^{-4}$, -0.7×10^{-4}), with a power law slope of −2.6 (Fig. 2). This represents a decrease in bending rigidity of a factor of ~4.0 from the intact condition. There was no measurable difference between DNase I-treated cells in the presence or absence of enzyme inhibitors.

Electron microscopy

In intact cells, the shaft of each OPC was ~1.5–2 μm in diameter, and the microtubules generally formed a square array with regularly interdigitated parallel actin filaments (Fig. 3). The ratio of actin filaments to microtubules in this

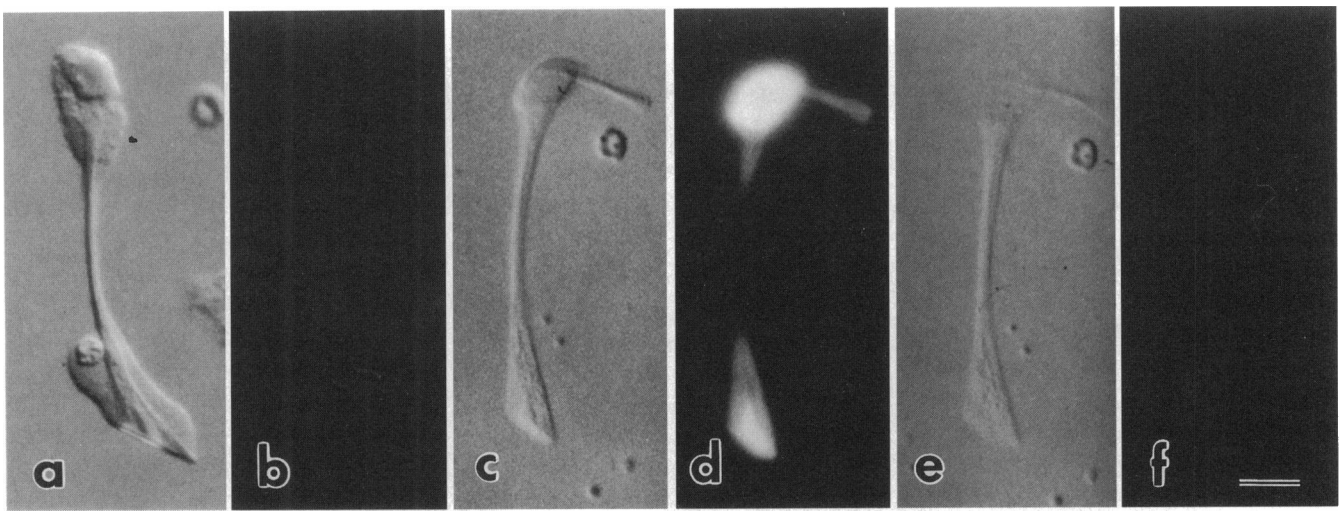

FIGURE 1 Intact cells (*a*) were much more refractive than punctured cells and both the nucleus and the plasma membranes were clearly defined. In some cases the apical microtubule process was folded downward against the main shaft of the cell. Intact cells excluded labeled phalloidin (*b*). The nucleus and plasma membrane were absent from punctured or Triton extracted cells (*c*) and the actin structures were strongly labeled with phalloidin (*d*). After treatment with DNase I (*e–f*) or high-intensity light excitation, most of this actin was removed and the apical plate and basal cone disappeared. Note that the microtubules in the apical process were not continuous with those of the shaft. Scale bar = 10 μm.

region was ~1:1, but in the apical and basal extremes the number of interdigitating actin filaments was greater and the square packing was not observed. Cross-links were observed between the microtubules and the actin filaments, and the number of microtubules was constant throughout the shaft. The total number of microtubules within an OPC varied linearly from ~1000 at the apical end of the cochlea to ~3000 in the basal end, in good agreement with a previous report (Kikuchi et al., 1991). When cross-links were visible in longitudinal sections, they occurred at regular intervals of ~10 nm between a given actin filament and adjacent microtubule along the microtubule length (Fig. 3 *d*).

In Triton-extracted cells, the square organization of microtubules disappeared, and the average density of microtubules was similar to the intact case at ~550 microtubules/μm^2. The ratio of interdigitated actin filaments to microtubules was reduced from 1:1 in intact cells to less than 1:10, with virtually a complete loss of visible cross-links in both longitudinal and transverse sections.

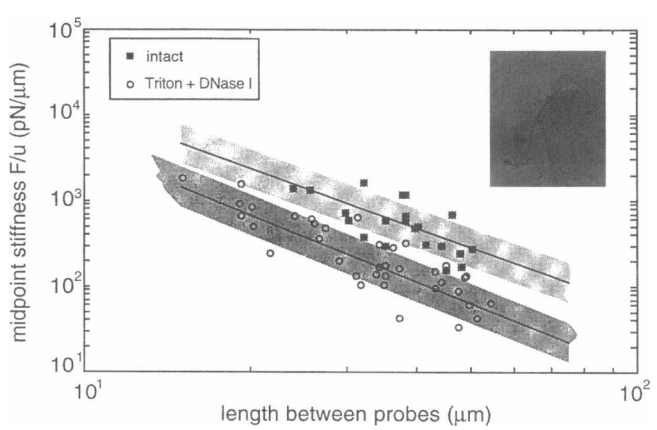

FIGURE 2 Stiffness at the midpoint of outer pillar cells under three-point bending. The data from cells treated with both 0.2% Triton X-100 and 0.1 mg/ml DNase I show a fourfold decrease in stiffness from the intact condition.

MODEL

If cross-linking between actin filaments and microtubules was responsible for the greater bending stiffness of intact OPCs, then the mechanism should involve a resistance of relative shear between individual microtubules. A beam theory is therefore required that includes both bending and shear deformation. Euler theory, the classical bending theory commonly used in engineering mechanics, does not include shear deformation. Timoshenko theory includes shear rotation of the midplane (Timoshenko, 1921), but it is only useful in a filament composite when the shear modulus is near the rigid limit. The electron microscopy of extracted cells shows very little cross-linking and suggests that the shear modulus may be small. A more appropriate theory capable of handling the full range of possible shear moduli is a layered beam system with interlayer slip. This has been developed analytically for three layer systems (Goodman and Popov, 1968) and for an arbitrary number of layers using approximate numerical methods (Steif and Trojnacki, 1993). In the following analysis, we further develop the analytical method to derive a simple model for shear slip bending in any number of beam layers. Fig. 4 shows the configuration and nomenclature used.

The aim of the model is to derive a system capable of converging to both a perfectly bonded bundle of microtubules and a perfectly frictionless unbonded bundle. The difference in these two bounds is the way in which individual microtubules are associated with each other. In the upper

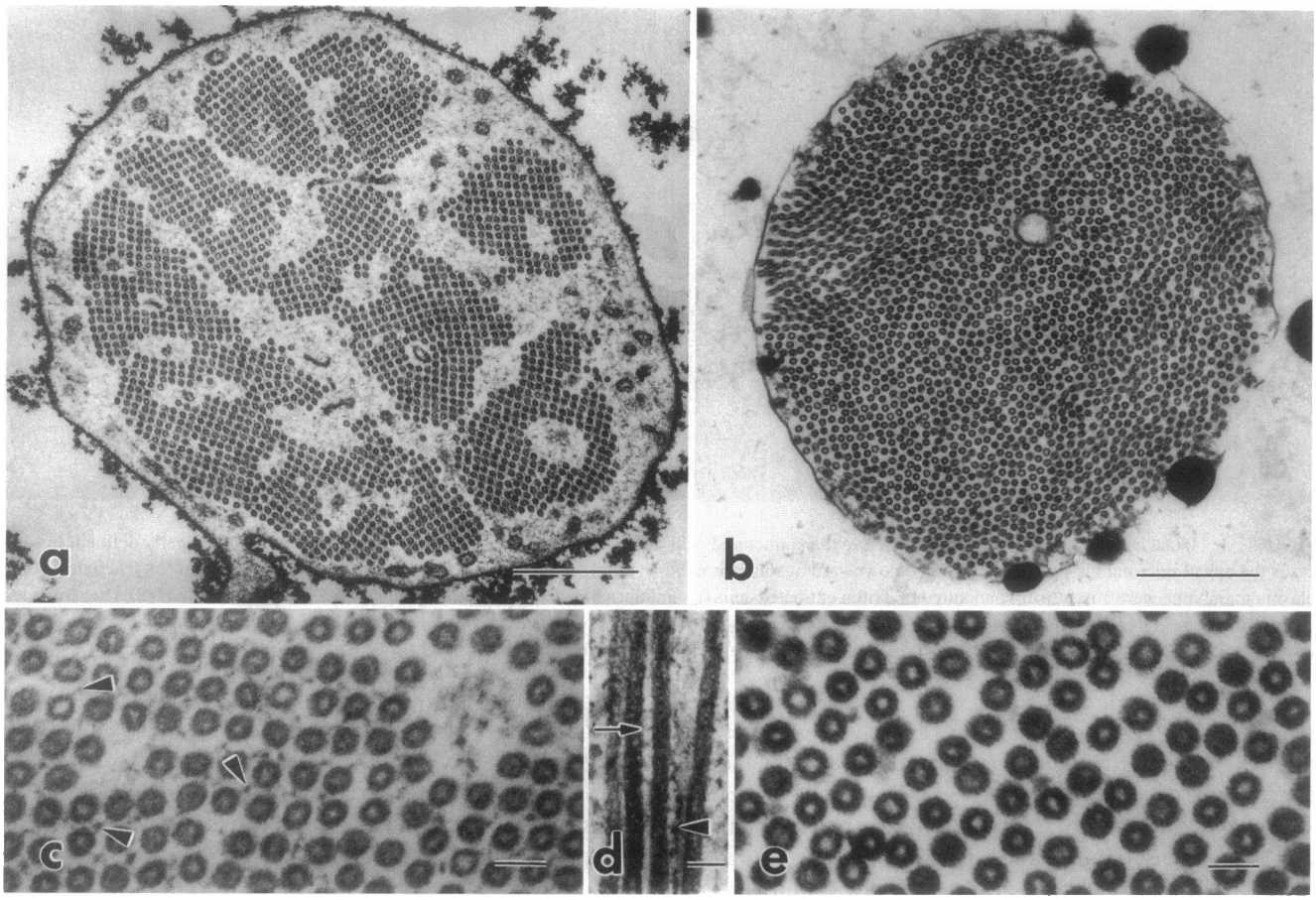

FIGURE 3 Electron micrographs of the cross-sectioned outer pillar cells, showing the distribution of microtubules in the central shaft under the experimental conditions that we have defined as intact (*a*) and extracted with 0.2% Triton X-100 (*b*). In intact cells (*c*) the microtubules formed a square array interdigitated with an equal number of actin filaments (*arrowheads*). In longitudinal section (*d*), cross-links were observed between actin filaments and microtubules (*arrowhead*) and more infrequently between microtubules (*arrow*). After extraction with Triton X-100 (*e*), most of the actin filaments and cross-links were removed and the square array disappeared. Scale bars = 0.5 μm (*a,b*) and 50 nm (*c–e*).

bound, each microtubule is rigidly cross-linked to its neighbor in such a way that no shear deformation between them is possible. In the lower bound there is negligible shear elasticity between microtubules, so that they are free to slide relative to each other, which results in a reduction in bending stiffness.

The classical Euler-Bernoulli expression used for the change in curvature in any beam layer in relation to the bending moment M within that layer is

$$\frac{\partial^2 w}{\partial x^2} = -\frac{M}{EI} \tag{1}$$

where w is the deflection, and the bending modulus EI is the product of the Young's modulus E and the moment of inertia I of a single layer. The total moment acting on the beam can be written as a sum of the moments in each layer plus the sum of the moments about the bundle center produced by the internal axial force F in each layer n:

$$M_{\text{applied}} = (2N + 1)M + 2\sum_{n=1}^{N} F_n nh \tag{2}$$

Describing the slip deformation, Δ, in terms of the difference in strain between layers,

$$\frac{\partial \Delta_n}{\partial x} = \frac{F_n - F_{n-1}}{AE} - \frac{Mh}{EI} \tag{3}$$

where A is the cross-sectional area of a layer. A linear constitutive law is assumed:

$$\frac{\partial \Delta_n}{\partial x} = \frac{t}{G}\frac{\partial \tau_n}{\partial x} \tag{4}$$

where τ is the shear stress, t is the interlayer spacing, and G is the shear modulus. Equilibrium on each layer relates the shear stress to the internal axial load, where h is the layer thickness:

$$\tau_n = \frac{1}{h(2N + 1)}\frac{\partial}{\partial x}\sum_{j=n}^{N} F_j \tag{5}$$

Two approximations are needed to make this system of equations consistent with the well-documented Kirchhoff approximation that plane sections remain plane. These also

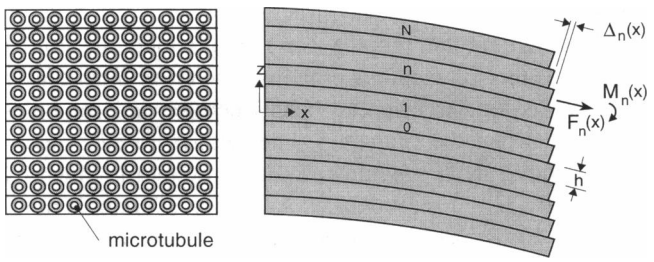

FIGURE 4 Transverse (*a*) and longitudinal (*b*) sections through the shear weak composite model consisting of $2N + 1$ layers. M is the bending moment within a layer, F is the internal extensional force, and h is the layer thickness. The system is symmetrical about the center layer. In bending, there is no force between microtubules that are equidistant from the neutral axis of deformation; therefore a row of microtubules is considered as a beam layer. For the average cell length of ~90 μm used in the experiments, the number of microtubules is ~2000. The number of layers is approximately the square root of the number of microtubules and therefore equals ~45 layers.

provide the point of departure from the exact three-layer analysis (Goodman and Popov, 1968). The first approximation is that the axial force F is distributed linearly in the z direction:

$$F_n = nF_1 \tag{6}$$

The second approximation is that the shear can be described by an average constant value similar to the shear correction factor used in Timoshenko theory:

$$\tau = \frac{K}{h(2N+1)}\frac{\partial F_1}{\partial x} \tag{7}$$

where K is defined as

$$K = \frac{1}{N}\sum_{n=1}^{N}\sum_{i=n}^{N} i \tag{8}$$

Equations 6 and 7 are combined with Eqs. 3–5 to arrive at the pair of coupled governing equations:

$$\frac{\partial^2 F_1}{\partial x^2} - \left(\frac{G}{tKhE} + \frac{2h^3G}{tKEI}\sum_{n=1}^{N} n^2\right)F_1 = -\frac{h^2G}{tKEI}M_{\text{applied}} \tag{9}$$

$$\frac{\partial^2 w}{\partial x^2} = \frac{1}{EI(2N+1)}\left(2hF_1\sum_{n=1}^{N} n^2 - M_{\text{applied}}\right) \tag{10}$$

For the three-point bending experiment, an applied load V at the cell center develops a moment on the left half of the beam of $M_{\text{applied}} = Vx/2$. Equation 9 is solved uniquely, by using the corresponding boundary conditions of $F = 0$ at $x = 0$ and $dF/dx = 0$ at $x = L/2$. Equation 10 is subsequently solved by using similar displacement boundary conditions of $w = 0$ at $x = 0$ and $dw/dx = 0$ at $x = L/2$. The displacement solution at the cell midpoint is given below, where β^2 is the term in parenthesis in Eq. 9:

$$w_{L/2} = -\frac{VL^3}{48EI(2N+1)} + \frac{Vh^3G\sum_{n=1}^{N} n^2}{tKE^2I^2(2N+1)}\left(\frac{L^3}{24\beta^2} - \frac{L}{2\beta^4} + \frac{\tanh \beta L/2}{\beta^5}\right) \tag{11}$$

The effect of increasing shear modulus on stiffness is shown in Fig. 5. Based on light and electron microscopy, the permeabilized and DNase I-treated cells are assumed to possess negligible shear resistance. This data is set as the lower limit, corresponding to 2000 individual uncoupled microtubules. Fitting an Euler theory cubic curve to the data gives a bending modulus of $EI = 7 \times 10^{-23}$ Nm^2 for an individual microtubule. Assuming that microtubules are homogeneous, with a moment of inertia based on an outer diameter of 30 nm and an inner diameter of 17 nm, gives $E = 2 \times 10^9$ Pa, which is in good agreement with published values (Gittes et al., 1993; Kurachi et al., 1995). Using a cross-link length of ~10 nm, the intact cell shear modulus value is $G = 10^3$ Pa. This shear resistance between microtubules in intact cells results in an increase in bending stiffness.

DISCUSSION

The average measured midpoint bending stiffness for undamaged, dissociated OPCs was 7×10^{-4} N/m. This value decreased to 2.7×10^{-4} N/m and then to 1.7×10^{-4} N/m, with partial and then complete loss of actin filaments and cross-links. These changes might have been due to loss of the plasma membrane, loss of actin filaments, a change in individual microtubule stiffness associated with the loss of MAPs, or loss of the cross-links between microtubules and

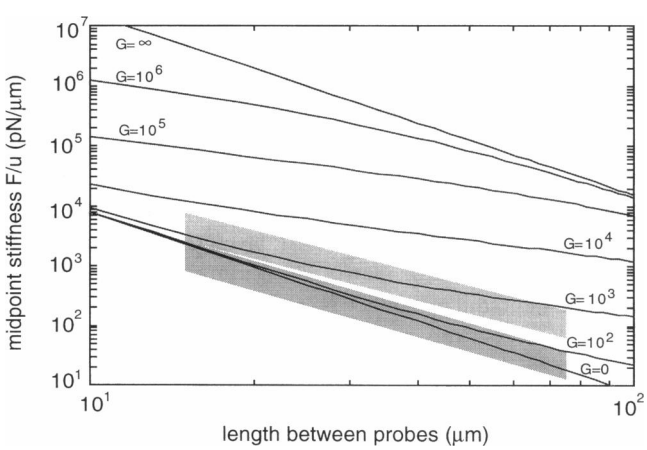

FIGURE 5 Results from the shear weak composite model. The solution converges to the unbonded and perfectly bonded limits, as given by Euler theory. The shaded lines show the average (± SD) experimental results for cells extracted with DNase I (*lower*) and for intact cells (*upper*). The best curve fit to the data occurs for $E = 2 \times 10^9$ Pa, with a shear modulus for intact cells of $G \approx 10^3$ Pa.

actin filaments. In this discussion we conclude that the fourfold change in stiffness is due to loss of cross-linking.

Plasma membrane

The plasma membrane is unlikely to contribute significantly to the change in stiffness. For a membrane resultant modulus of 10^{-5} N/m (Mohandas and Evans, 1994) and a cell diameter of less than 2 μm, the contribution to bending stiffness would be 3×10^{-23} Nm^2. Thus the membrane is expected to contribute less than 0.1% of the total bending stiffness of the pillar cell. There was little difference between punctured cells, where some residual membrane may have remained, and detergent-extracted cells, where it was likely to be completely removed. In addition, there would not have been any further loss of membrane to accompany the change in stiffness when cells were treated with DNase I. Finally, cells were checked to ensure that they were not stuck to the slide, so that a change in boundary condition was eliminated as the cause of the stiffness change.

Actin

The loss of actin filaments is also unlikely to contribute directly to the measured decrease in bending stiffness. Whereas the Young's modulus of actin (~3 GPa) is similar to that of microtubules (Gittes et al., 1993; Kojima et al., 1994), the diameter of an actin filament is only about one-fifth that of microtubules, leading to a moment of inertia ~100 times smaller. Therefore, the bending rigidity of actin contributes at most 1% of the cell bending stiffness. The role of actin is more likely to facilitate cross-linking organization (Pollard et al., 1984), as suggested by the dependence of microtubule square packing on the 1:1 ratio of actin filaments to microtubules.

Cross-links

The measured changes in bending stiffness can be explained in terms of the cross-links. The value of the bending modulus of $EI = 7 \times 10^{-23}$ Nm^2 is greater than that reported for individual microtubules with only 13 protofilaments (Gittes et al., 1993; Kurachi et al., 1995; Vernier et al., 1994; Kurz and Williams, 1995). However, considering the larger diameter and moment of inertia, the Young's modulus for 15 protofilament microtubules is $E = 2$ GPa, which is very similar to recent reports for 13 protofilament microtubules. This agreement validates the usage of DNase I-treated cells as the baseline of the model for un-cross-linked microtubules.

Cross-links could theoretically produce a dramatic increase in bending stiffness by providing shear resistance between microtubules. In OPCs, they appear to increase stiffness by a factor of 4, which may make a significant difference to the cell. However, this is only a fraction of the full potential, as shown in Fig. 5, where all of the experimental data lie close to the lower limit. This is consistent with what we know of the structure of the cross-links in OPCs, assuming that they have a Young's modulus similar to that of other filamentous proteins. The cross-links can be modeled as regularly spaced beams between microtubules that bend when the filaments slide relative to each other. The effective shear modulus of such a system is given by the formula $G = E\pi d^4/(64bL^3)$. Assuming a Young's modulus $E = 10^7$ Pa, a cross-link length $L = 10$ nm, a cross-link diameter $d = 3$ nm, and spacing along the microtubule $b = 10$ nm, the shear modulus is $\sim 10^3$ Pa, very similar to our experimental results. Thus the measured decrease in cell stiffness is entirely consistent with the progressive extraction of cross-links that interconnect the microtubules via the actin filaments.

The results from the electron microscopy support the view that the microtubules are cross-linked via the actin filaments. Although we have clearly removed the cross-linking in the presence of detergent, we have not established that the cross-link MAPs are formed by the 205-kD MAP described by Oshima et al. (1992). An antibody against this protein (kindly supplied by Prof. N. Hirokawa) labeled pillar cells both before and after treatment with detergent (data not presented), suggesting either that the 205-kDa MAP is independent of the cross-links or that it is merely disconnected from the actin.

Various MAPs are known to form cross-links and facilitate bundle formation, but there are conflicting reports on whether or not they change the bending rigidity of individual microtubules. In Kurz and Williams (1995), a group of MAPs were shown to have no effect on the stiffness of isolated individual microtubule polymerized in vitro. In contrast, Felgner et al. (1996) found that MAPs added to the bathing solution after microtubule polymerization did increase the bending stiffness of individual microtubules. It is unlikely that the difference seen in our results is due to changes in the stiffness of individual microtubules. The small change in slope found in the stiffness-to-length curves (Figs. 3 and 5) is consistent with the cross-link model, but would not occur for a stiffness change in individual microtubules. Furthermore, it is unlikely that MAPs lying along the length of the microtubules and then removed during the extraction process can cause a significant change in bending stiffness. This is based on the diameter of known MAPs and the negligible increase they therefore provide to the moment of inertia.

The proposed mathematical model incorporates as distinct elements the material properties of both microtubules and their cross-links, based on experimental measurements we have made from auditory pillar cells. Given some elementary morphological data, the model can be applied to any bundled cytoskeletal polymer to provide estimates of the mechanical properties of cells that cannot be measured directly. In the mammalian inner ear, this includes Deiter's cells, which are similar structurally to the pillar cell, but which are extremely difficult to dissociate intact from the sensory epithelium.

This work was supported by the Wellcome Trust and a Royal Society Research Fellowship to MCH.

REFERENCES

Angleborg, C., and H. Engström. 1972. Supporting elements in the organ of Corti. *Acta Otolaryngol. Suppl. (Stockh.).* 301:49–60.

Arima, T., T. Uemura, and T. Yamamoto. 1986. Cytoskeletal organization in the supporting cell of the guinea pig organ of Corti. *Hear. Res.* 24:169–175.

Felgner, H., R. Frank, and M. Schliwa. 1996. Flexural rigidity of microtubules measured with the use of optical tweezers. *J. Cell Sci.* 109: 509–516.

Gittes, F., B. Mickey, J. Nettleton, and J. Howard. 1993. Flexural rigidity of microtubules and actin filaments measured from thermal fluctuations in shape. *J. Cell Biol.* 120:923–934.

Goodman, J. R., and E. P. Popov. 1968. Layered beam systems with interlayer slip. *Proc. Am. Soc. Civil Eng. J. Struct. Div.* 2535–2547.

Griffith, L. M., and T. D. Pollard. 1982. The interaction of actin filaments with microtubules and microtubule-associated proteins. *J. Biol. Chem.* 257:9143–9151.

Iurato, S. 1961. Submicroscopic structure of the membranous labyrinth. *Z. Zell. Mikrosk. Anat.* 53:259–298.

Kikuchi, T., T. Takasaka, A. Tonosaki, Y. Katori, and H. Shinkawa. 1991. Microtubules of guinea pig cochlear epithelial cells. *Acta Otolaryngol. (Stockh.).* 111:286–290.

Kojima, H., A. Ishijim, and T. Yanagida. 1994. Direct measurements of stiffness of single actin filaments with and without tropomysin by in vitro nanomanipulation. *Proc. Natl. Acad. Sci. USA.* 91:12962–12966.

Kurachi, M., M. Hoshi, and H. Tashiro. 1995. Buckling of a single microtubule by optical trapping forces: direct measurement of microtubule rigidity. *Cell Motil. Cytoskel.* 30:221–228.

Kurz, J. C., and R. C. Williams. 1995. Microtubule-associated proteins and the flexibility of microtubules. *Biochemistry.* 34:13374–13380.

Lazarides, E., and U. Lindberg. 1974. Actin is the naturally occurring inhibitor of deoxyribonuclease 1. *Proc. Natl. Acad. Sci. USA.* 71: 4742–4746.

MacRae, T. H. 1992. Microtubule organization by cross-linking and bundling proteins. *Biochim. Biophys. Acta.* 1160:145–155.

Mohandas, N., and E. Evans. 1994. Mechanical properties of the red blood cell membrane in relation to molecular structure and genetic defects. *Annu. Rev. Biophys. Biomol. Struct.* 23:787–818.

Oshima, T., S. Okabe, and N. Hirokawa. 1992. Immunocytochemical localization of 205 kDa microtubule-associated protein (205 kDa MAP) in the guinea pig organ of Corti. *Brain Res.* 590:53–65.

Pollard, T. D., S. C. Selden, and P. Maupin. 1984. Interaction of actin filaments with microtubules. *J. Cell Biol.* 99:33s–37s.

Saito, K., and K. Hama. 1982. Structural diversity of microtubules in the supporting cells of the sensory epithelium of the guinea pig organ of Corti. *J. Electron Microsc. (Tokyo).* 31:28–281.

Slepecky, N., and S. C. Chamberlain. 1983. Distribution and polarity of actin in inner ear supporting cells. *Hear. Res.* 10:359–370.

Steif, P. S., and A. Trojnacki. 1993. Bending stress enhancement in materials with limited shear resistance. I. Slipping layers model. *Int. J. Solids Struct.* 30:1355–1368.

Timoshenko, S. P. 1921. On the correction for shear of the differential equation for transverse vibrations of prismatic bars. *Philos. Mag.* 41: 744–747.

Tolomeo, J. A., C. R. Steele, and M. C. Holley. 1996. Mechanical properties of the lateral cortex of mammalian auditory outer hair cells. *Biophys. J.* 71:421–429.

Vernier, P., A. C. Maggs, M. Carlier, and D. Pantaloni. 1994. Analysis of microtubule rigidity using hydrodynamic flow and thermal fluctuations. *J. Biol. Chem.* 269:13353–13360.